Journal of the European Ceramic Society 23 (2003) 1157–1166
www.elsevier.com/locate/jeurceramsoc

Effect of PMN modification on structure and electrical response of xPMN–(1−x)PZT ceramic systems

Vladimír Koval[a,*], Carlos Alemany[b], Jaroslav Briančin[a], Helena Bruncková[a], Karol Saksl[a]

[a] *Institute of Materials Research, Slovak Academy of Sciences, Watsonova 47, 04353 Košice, Slovakia*
[b] *Instituto de Ciencia de Materiales de Madrid, CSIC, Cantoblanco, 28049 Madrid, Spain*

Received 16 May 2002; accepted 28 July 2002

Abstract

The structural and electrical properties of xPb($Mg_{1/3}Nb_{2/3}$)O_3–(1−x)Pb(Zr,Ti)O_3 ternary ceramic system with the composition near to the morphotropic phase boundary (MPB) and of xPb($Mg_{1/3}Nb_{2/3}$)O_3–(1−x)Pb($Zr_{0.47}Ti_{0.53}$)O_3 ceramics were investigated as a function of the Pb($Mg_{1/3}Nb_{2/3}$)O_3 (PMN) content by scanning electron microscopy (SEM), X-ray diffraction (XRD), dielectric and piezoelectric spectroscopy and polarization-electric field measurement technique. Studies were performed on the samples prepared by a columbite precursor method for $x=0.125$, 0.25 and 0.5. Room temperature SEM investigations revealed common trends in the grain structure with increasing PMN content. XRD analysis demonstrated that with increasing PMN content in xPb($Mg_{1/3}$ $Nb_{2/3}$)O_3–(1−x)Pb($Zr_{0.47}Ti_{0.53}$)O_3, the structural change occurred from the tetragonal to the pseudocubic phase at room temperature. Changes in the dielectric and ferroelectric behavior were then related to these structural trends and further correlated with the piezoelectric properties. The results of ferroelectric hysteresis measurements, in conjunction with dielectric spectroscopy, demonstrated an intermediate, relaxor-like behavior between normal and relaxor ferroelectrics in the solid solution system, depending on the PMN content.

Keywords: Dielectric properties; Ferroelectric properties; Grain size; Piezoelectric properties; PMN–PZT

1. Introduction

Undoubtedly nowadays, ferroelectric lead zirconate titanate (PZT) compositions belong to the materials destined besides the classical piezoelectric using also for microelectromechanical systems (MEMS) applications because their excellent piezoelectric and pyroelectric properties are well-known and defined. Moreover, they are being produced as good-quality, polycrystalline thin and thick films by a variety of forming methods.[1,2] However, these materials exhibit large dielectric and electromechanical hysteresis when operating at high fields.[3] It makes difficulties to control the electromechanical response of MEMS devices based on ferroelectric PZT thin films.

Alternative materials that also offer some of the same desirable qualities are electrostrictive materials. Recently, a number of electrostrictive ferroelectrics have been obtained on the basis of complex lead niobates of Pb($B'_{1/3}$ $Nb_{2/3}$)O_3-type (where B′–Mg^{2+}, Zn^{2+}, Ni^{2+}),[4–7] which has risen an interest in the properties of multicomponent ceramic solid solutions because of a very interesting combination of large electrostrictive strains and a minimal or negligible hysteresis in the strain-field dependence.

Experimentally it has been substantially reported that lead-based 1:2 complex mixed perovskite ferroelectrics are composed of paraelectric matrix and non-stoichiometricaly 1:1 short-ordered nanopolar regions.[8] It is generally accepted that the compositional fluctuations are responsible for unusual relaxor behavior of these materials.[9,10] The studies by neutron and X-ray diffraction[11] completed by dielectric spectroscopy[12] on PMN and related materials have revealed that either the peak of the dielectric permittivity or the peak of the dielectric absorption does not correlate with any macroscopic phase transition in relaxors. The real macroscopic phase transition of the first order to a rhombohedral phase has been detected by cooling PMN in a dc field higher than a treshold electric field.[13]

* Corresponding author. Fax: +421-55-6337108.
E-mail address: koval@imrnov.saske.sk (V. Koval).

0955-2219/03/$ - see front matter
PII: S0955-2219(02)00281-9

An interesting family of materials is solid solutions of a PMN relaxor and a ferroelectric lead titanate (PT) and/or lead zirconate (PZ).[4,5] Their temperature of dielectric permittivity maximum (T_m), and thus an operation range are controlled by the PT and PZ content, respectively. Furthermore, a substitution on cationic sites, without changing the Mg/Nb ratio, may induce change in the degree of ordering. As a result, T_m is increased and the threshold field strength value needed to induce a macroscopic symmetry change is lowered to zero at the temperature below T_m. A spontaneous (zero-field) relaxor to normal ferroelectric phase transition has been reported for these complex compounds. Using X-ray diffraction analyses, dielectric and piezoelectric measurements, Ouchi et al.[14] established a phase diagram of ternary PMN–PZ–PT solid solution system. High values of the dielectric permittivity and radial coupling factor have been reported for the composition near the morphotropic phase boundary (MPB). Tsotsorin et al.[15] investigated the dielectric and electromechanical properties of $(1-x)$PMN-xPb$(Zr_{0.53}Ti_{0.47})O_3$ ceramic solid solutions and reported that the dielectric peaks in temperature dependence of the relative dielectric permittivity and loss tangent are transformed from a wide diffused shape to a more sharp form with increasing of ferroelectric component PZT in the solid solution. The electrostriction coefficients exhibited maximum for the composition with $x=0.11$ and their magnitude decreased with the temperature increasing from T_m.

The references on the solid solution between PMN and PZT, at least, do not discuss the phase-pure quality of the investigated ceramics regarding to the presence of pyrochlore phase. In addition, there have been any common studies done on the dielectric and ferroelectric behavior and structural characterization, and the relationship between them for PMN–PZT ferroelectric ceramics. As an extension of the research on the PMN–PZT system, we present here results of the study of structural, dielectric, ferroelectric and piezoelectric properties of the xPMN–$(1-x)$PZT solid solution ceramic system prepared by a columbite precursor method. Discussion includes the PMN substitution into PZT and its effect on the grain size, crystal structure and electrical response of ceramics. The results are reported for two series of xPMN–$(1-x)$PZT materials with $x=0.125$, 0.25 and 0.5; the compositions near to the morphotropic transformation and ceramics with a Ti:Zr ratio equals to 53:47.

2. Experimental procedure

2.1. Sample preparation and structural characterization

The following compositions of xPMN–$(1-x)$PZT solid solution system were used in this study:

1. The MPB compositions (refereed to A-series materials hereafter) and can be represented by: $0.125Pb(Mg_{1/3}Nb_{2/3})O_3$–$0.435PbTiO_3$–$0.44PbZrO_3$ abbreviated as 0.125PMN–PZT(50:50), $0.25Pb(Mg_{1/3}Nb_{2/3})O_3$–$0.4PbTiO_3$–$0.35PbZrO_3$ abbr. 0.25PMN–PZT(53:47), $0.5Pb(Mg_{1/3}Nb_{2/3})O_3$–$0.375PbTiO_3$–$0.125PbZrO_3$ abbr. 0.5PMN–PZT(75:25).
2. The compositions with a Ti:Zr ratio equals to 53:47 (refereed to B-series materials hereafter) as: $0.125Pb(Mg_{1/3}Nb_{2/3})O_3$–$0.465PbTiO_3$–$0.41PbZrO_3$ abbr. 0.125PMN–PZT(53:47), $0.25Pb(Mg_{1/3}Nb_{2/3})O_3$–$0.4PbTiO_3$–$0.35PbZrO_3$ abbr. 0.25PMN–PZT(53:47), $0.5Pb(Mg_{1/3}Nb_{2/3})O_3$–$0.265PbTiO_3$–$0.235PbZrO_3$ abbr. 0.5PMN–PZT(53:47), and pure $Pb(Mg_{1/3}Nb_{2/3})O_3$.

A columbite precursor route was adopted for the synthesis of stoichiometric powders. More details of the synthesis of $MgNb_2O_6$ precursor powder can be found in Ref.[16] The mixture of considered amounts of reagent-grade oxide powders of Pb_3O_4, ZrO_2, TiO_2 and $MgNb_2O_6$ was wet ball-milled (Fritsch, model Pulverisette) in a stoichiometric ratio, dried and then calcined at 850 °C for 2 h in alumina crucible. After that, the reacted material was additionally ball-milled to ensure a fine particle size before sintering. The dried powder was axially pressed into disks of 13 mm in diameter and about 2 mm in thickness. The green pellets were sintered for 2 h at 1200 °C on a Pt plate. To limit PbO loss during the high-temperature sintering of material, an atmosphere powder consisting of a mixture of $PbZrO_3$ and ZrO_2 powders was placed inside the covered alumina crucible.

The apparent densities of the sintered samples were measured by Archimedes's method and computed from the sample weight in air, in water, with adsorbed water in air, and the density of the water used. These data were compared with the theoretical density as calculated from XRD measurements.

The crystal structure and lattice parameters were determined from XRD (Philips, model X'Pert Pro) patterns, that were recorded with CuK_α radiation ($\lambda=0.15405$ nm) at room temperature over the angular range of $20^\circ \leqslant 2\theta \leqslant 60^\circ$ by step of 0.015°. The volume percentage of perovskite phase in each composition was calculated using the following qualitative equation:[16]

$$\%\ \text{perovskite} = \frac{(I_{110})_{\text{perov}}}{(I_{110})_{\text{perov}}+(I_{222})_{\text{pyro}}} \times 100\%,$$

where (I_{110}) and (I_{222}) are the major X-ray peak intensities for a perovskite phase and a pyrochlore phase, respectively.

The developed ceramic microstructure was analyzed under scanning electron microscopy (SEM; Tesla, model BM 340). Polished sections of the fractured surfaces of sintered pellets were chemically etched in a solution containing 0.5% HF and 5% HCl. After drying, the disk samples were Au coated by sputtering (Jeol, model JFC-1100). The average grain size was determined by the linear intercept method.

For the property measurement, the sintered disks were lapped step-by-step with SiC papers to approximately 0.2 mm thickness, and then cleaned with methanol using an ultrasonic cleaner. The major faces of specimens were electroded by applying Ag paste, and fired at 830 °C for 30 min. The labeling and fundamental characteristics of the samples are given in Table 1.

For piezoelectric characterization, the samples were poled in a silicone oil bath at a temperature of 110 °C by applying a dc field of 30 kV/cm for 30 min and field-cooled to room temperature.

2.2. Dielectric characterization

Dielectric measurements were carried out on an automated system, whereby a low-frequency impedance analyser (Hewlett-Packard, model HP 4192A) was controlled by a computer. The temperature dependencies of the relative dielectric permittivity, as calculated from the capacitance and size of the sample, and the dissipation factor were measured on cooling continuously at several frequencies between 100 Hz and 1 MHz. The specimens were placed in a small home-made furnace, specifically equipped for such measurement, that could be operated over a temperature range of room temperature and 450 °C. The temperature was measured using a voltage meter (Keithley, model 177 Microvolt DMM meter) with a chromel-alumel thermocouple mounted near the surface of the sample and controlled to within ± 1 °C using a home-made temperature controller. Before each cooling run, the sample was first heated up to 450 °C and then cooling run was performed at the rate of 5 °C/min outside of the phase transition temperature and of 0.5 °C/min around the dielectric permittivity maximum.

2.3. Piezoelectric characterization

After 24 h aging at room temperature, complex impedance patterns were obtained using the above mentioned impedance analyzer, which can cover a frequency range between 5 Hz and 13 MHz. The four-terminal-pair configuration was used to improve the measurement accuracy. Before the measurement, a standard compensation routine was performed to reduce the effects of the errors sources, such as stray capacitance, lead, and contact resistance. The evaluation of piezoelectric properties was done by an iterative procedure of resonance-antiresonance method proposed by C. Alemany et al.[17] The piezoelectric d_{33} constant was measured at 100 Hz by a piezo d_{33}-meter (Channel product, model Berlincourt d_{33}-meter).

2.4. Hysteresis loop measurements

The ferroelectric hysteresis (P–E) loops were characterized by using a computer controlled, virtual ground circuit. Peak-to-peak voltages were applied to the samples by a bipolar amplifier (Kepco, model BOP 1000M), in which input signals were generated by a wave-form signal generator (Hewlett-Packard, model HP 3325B). Output signals from the samples were registered by a home-made integrator and then processed by the computer. The cycling frequency was 0.01 Hz and the maximum switching field applied on the sample was 1000 V. Specimens were immersed in a silicon oil bath.

3. Results and discussion

3.1. Ceramic properties

The structural parameters of xPMN–(1−x)PZT materials as a function of different PMN content and Ti:Zr ratio are collected in the second part of Table 1. The sintered densities are better than 97% of theoretical values. While the effect of $Mg_{1/3}Nb_{2/3}$ concentration on the density of A-series materials was almost negligible

Table 1
Composition, density and structural parameters of xPMN–(1−x)PZT ceramics

	Sample	x	Ti:Zr	$\rho \times 10^3$ [kg/m^3]	GS $\times 10^{-6}$ [m]	$a \times 10^{-10}$ [m]	$c \times 10^{-10}$ [m]	c/a tet.	v %
A-series materials	PMN1	0.125	50:50	7.80	2.0	4.06	4.14	1.02	100
	PMN2	0.25	53:47	7.73	0.9	4.03	4.11	1.02	90
	PMN3	0.5	75:25	7.83	1.0	4.04	4.05	1.00	84
B-series materials	PMN1T	0.125	53:47	7.86	1.0	4.03	4.12	1.02	100
	PMN2M	0.25	53:47	7.75	1.6	4.03	4.11	1.02	90
	PMN3P	0.5	53:47	7.71	0.9–2.5	4.06	–	–	70
	PMN	1.0	–	7.86	2.5	4.03	–	–	81

x—PMN content, ρ—sintered density, GS—average grain size, a, c—tetragonal lattice parameters, v—volume fraction of perovskite phase.

($\rho \approx 7.8$ g/cm^3), in B-series materials the density of sintered samples decreased with increasing PMN content.

Fig. 1 shows the X-ray diffraction patterns of B-series materials as a function of PMN content at room temperature. From the figure it is apparent that PMN1T is a single-phase material with a perovskite structure exhibiting tetragonal symmetry. Morphotropic compositions, such as PMN2M and other A-series materials exhibited an overlapping of the diffraction lines and the presence of a triplet at (h00) peaks, as representatively shown in Fig. 1 for PMN2M. These features are obviously associated to the materials, in which two or more phases coexist. The XRD pattern of PMN3P displays a pseudocubic partially distorted perovskite structure. No recognizable splitting of X-ray lines can be seen. Even though a columbite method was used, the volume percentage of the perovskite phase decreases for both A- and B-series materials as the amount of PMN increases (see Table 1). From Fig. 1 it is clear, that the major X-ray peak intensity for a pyrochlore phase (222) gradually increases as the mole percentage of PMN (x) increases. A decreasing of the bulk density in B-series materials could be therefore correlated with an increasing pyrochlore phase, that originates from the decomposition of perovskite phase during sintering process. The lattice parameters were calculated by a least square method from the X-ray diffraction angles and are listed together with a tetragonal distortion in Table 1. No substantial effect of the enhanced lattice disorder by an introduction of Mg and Nb ions has been observed in ternary PMN–PZT system, $(c/a)_t \sim 1.02$.

Fig. 2 shows scanning electron micrographs of polished, chemically etched surfaces of xPMN–$(1-x)$PZT with the composition near the MPB and of $Pb(Mg_{1/3}Nb_{2/3})O_3$ ceramics (Fig. 2d). The micrographs reveal that the PMN modification reduces the rate of grain growth. The average grain size decreased from 2.2 μm for $x = 0.125$ to approximately 1 μm for the composition with $x = 0.5$.

Microstructural features of xPMN–$(1-x)$PZT ceramics with Ti:Zr = 53:47 sintered at 1200 °C for 2 h are presented in Fig. 3. As shown in the micrographs, the solid solution ceramic systems exhibit a fine grain structure. It should be noticed, that the ceramic material

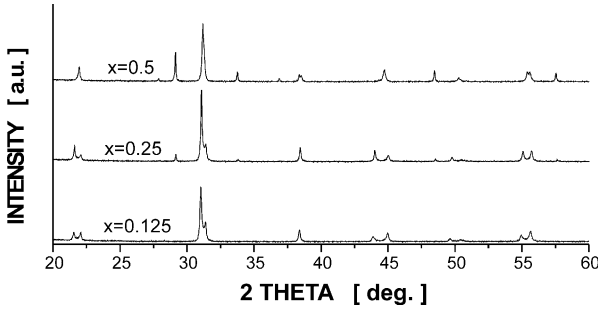

Fig. 1. Room-temperature X-ray diffraction patterns for $x Pb(Mg_{1/3}\ Nb_{2/3})O_3$ –$(1-x)Pb(Zr_{0.47}Ti_{0.53})O_3$ ceramics.

with a high-PMN content ($x = 0.5$) showed a very heterogeneous microstructure (Figs. 2c and 3b) with a large amount of secondary pyrochlore phase, as XRD patterns indicated. Cubic particles of the pyrochlore phase were observed at the matrix grain boundaries.

3.2. Dielectric properties

Fig. 4 shows the weak-field relative dielectric permittivity dependency on temperature measured at 1, 100 and 1000 kHz on cooling for the ceramic samples of xPMN–$(1-x)$PZT system ($x = 0.125$, 0.25, 0.5) with the composition near to the MPB (a) and with a Ti:Zr = 53:47 (b). In A-series materials (PMN1, PMN2, PMN3), the broadness of dielectric permittivity peak increases with increasing PMN content. Since the temperature of the dielectric permittivity maximum of PMN is ~ -8 °C, the dielectric permittivity peak temperature for all investigated compositions decreased as the molar fraction of PMN increased. However, between the dielectric behavior of A- and B-series materials appreciable changes in the dielectric peak were observed from the view-point of the PMN modification effect. While the maximum dielectric permittivity (ε_m) decreases from 25 500 for PMN1 to 3000 for PMN3 due to a change in Ti:Zr ratio, those of B-series materials monotonically increase from 4700 for PMN1T to 6700 for PMN3P. An increasing of ε_m may be related to a high dielectric permittivity of PMN ($\varepsilon_m \approx 7000$), and thus one can expect that the dielectric permittivity maximum of the xPMN–$(1-x)Pb(Zr_{0.47}Ti_{0.53})O_3$ solid solution system is controlled by the PMN content. Except the PMN3P ceramics, the samples of both series showed obvious dielectric behavior of the ferroelectrics with a diffuse phase transition (DPT). Although the absolute values of ε_m change with frequency, the transition temperature is not shifted as for relaxors. For the composition of morphotropic transformation of PMN2 and PMN3, below the dielectric permittivity maximum relaxor-like characteristics were found, as representatively illustrated in Fig. 5. With decreasing temperature, the loss tangent shows only very small decrease and its value is much higher than that above the critical temperature. The characteristic features of relaxor ferroelectrics were observed for 0.5 PMN–PZT(53:47). Considerable broadening of $\varepsilon_r(T)$ curve and the frequency dependence of diffuse phase transition (T_m) ascribed to the dynamics of polar nanodomains can be seen in Fig. 6. The peaks in the value of real part (ε_r) and imaginary part (ε'') of the complex dielectric permittivity both move towards a higher temperature as the frequency is increased.

From temperature-frequency-dependent data of the dielectric response of B- compositional series materials, it would appear that with increasing PMN content, phases continuously change from ferroelectric ($x = 0.125$) to relaxor ($x = 0.5$) through relaxor-like state ($x = 0.25$).

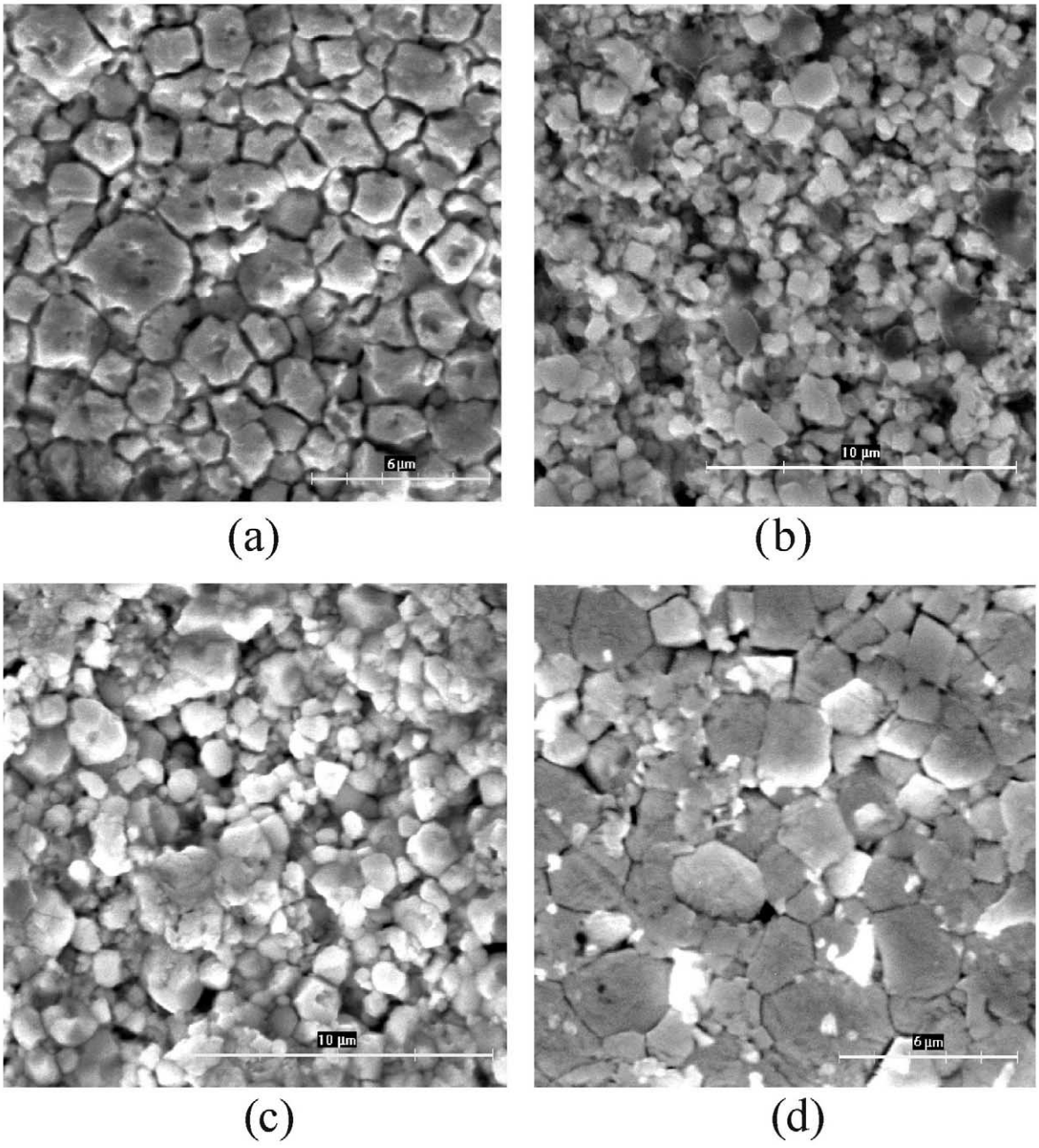

Fig. 2. SEM micrographs of xPMN–(1−x)PZT ceramic samples with the composition near to the MPB. (a) $x=0.125$, (b) $x=0.25$, (c) $x=0.5$, (d) $Pb(Mg_{1/3}Nb_{2/3})O_3$.

3.3. Ferroelectric properties

A sequence of polarization (P–E) hysteresis loops for the xPMN–(1−x)PZT ceramics with the composition in the vicinity of morphotropic transformation and various PMN content are illustrated in Fig. 7. It is evident that the shapes of P–E loops differ between the MPB compositions with x. The polarization loop of PMN1 is well developed showing a large remanent polarization at zero field. The hysteresis loop has a typical "square" form stipulated by switching of a domain structure in an electrical field, which is typical of a phase that contains long-range cooperation between dipoles. That is characteristic of a ferroelectric micro-domain state. The phase of PMN1 at room temperature is confirmed to be ferroelectric.

From the fully saturated loops, the remanent polarization P_r and coercive field E_c were determined. The values of P_r and E_c for PMN1 are 35.6 μC/cm^2 and 8.1 kV/cm, respectively, whereas for PMN2 the remanent polarization P_r is only 3.3 μC/cm^2, less than one tenth of that for PMN1. By moving through the MPB to the compositions with a higher PMN content, the dielectric P–E curves became nonlinear "slim" hysteresis loops

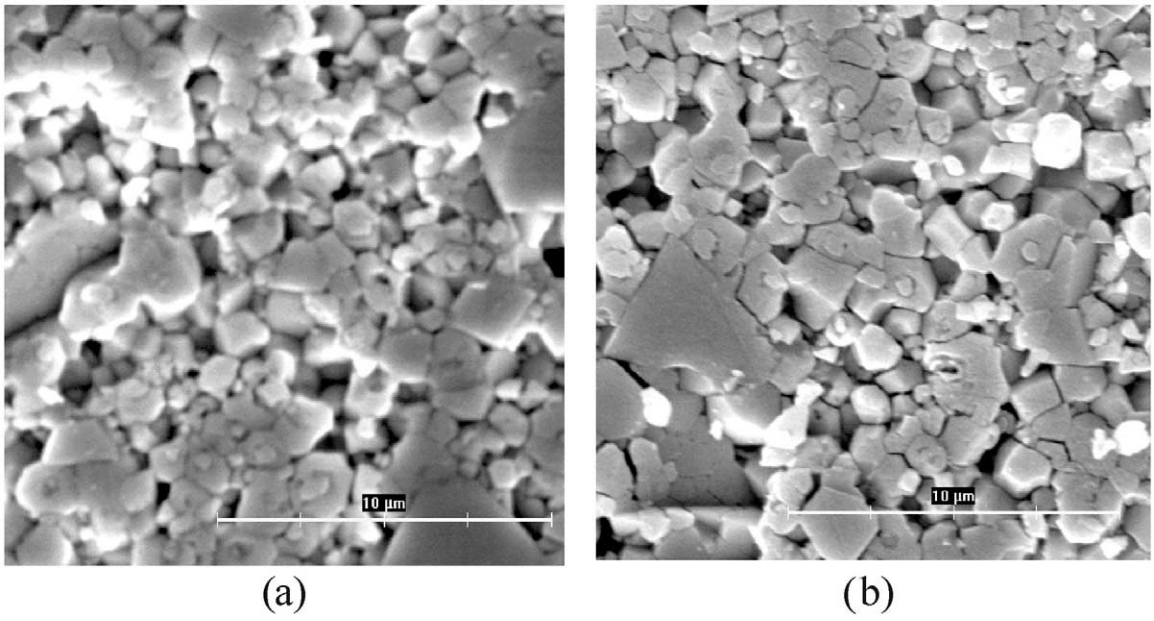

Fig. 3. SEM micrographs of xPb($Mg_{1/3}Nb_{2/3}$)O_3–(1−x)Pb($Zr_{0.47}Ti_{0.53}$)O_3. (a) $x=0.125$, (b) $x=0.5$.

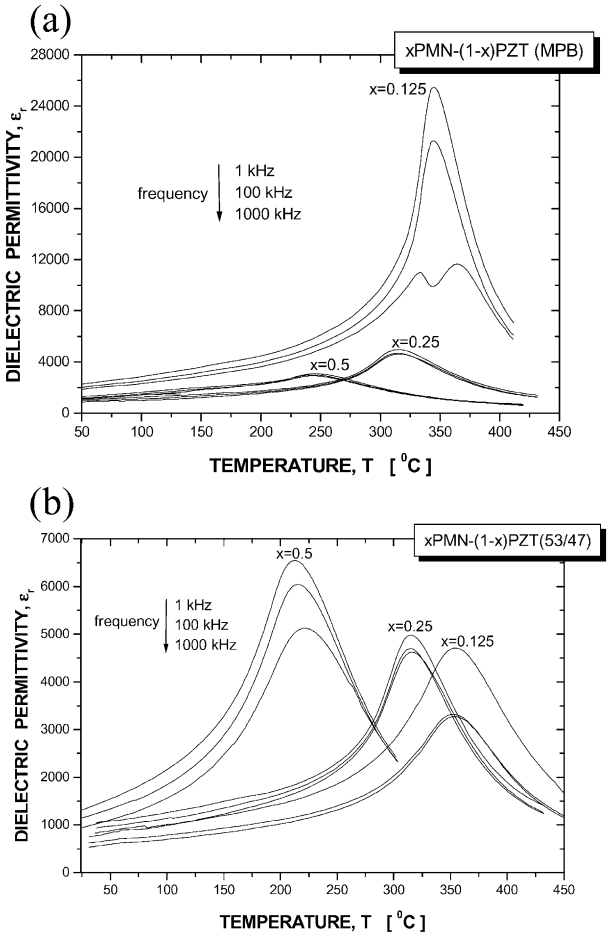

Fig. 4. Temperature dependence of the relative dielectric permittivity measured at 1, 100 and 1000 kHz on cooling for xPMN–(1−x)PZT ceramics. (a) MPB compositions, (b) compositions with a ratio Ti:Zr of 53:47.

characteristic of the suppressed ferroelectric interaction. The loop in Fig. 7b and Fig. 7c rather implies the coexistence of polar microdomains and macroscopical ferroelectric domains in PMN2 and PMN3, respectively.

A series of hysteresis loops for the MPB compositions of xPMN–(1−x)PZT at 25 °C and 100 °C is shown in Fig. 8. As we can see from Fig. 8, the coercive field, which can be identified as the intercept of the loop and $P=0$, is a strong function of temperature. The coercive field and also polarization for the all studied MPB compositions decreases with temperature.

The development of ferroelectric loop of PMN sample upon a change in temperature is shown in Fig. 9. The nonlinear "slim" hysteresis loop can be seen at 25 °C, which is characteristic of the absence of a long-range

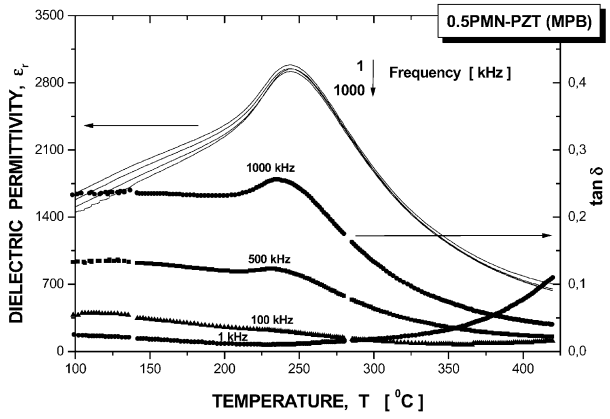

Fig. 5. Dielectric response of 0.5Pb($Mg_{1/3}Nb_{2/3}$)O_3–0.5Pb($Zr_{0.25}Ti_{0.75}$)O_3 ceramics measured at 1, 100, 500 and 1000 kHz.

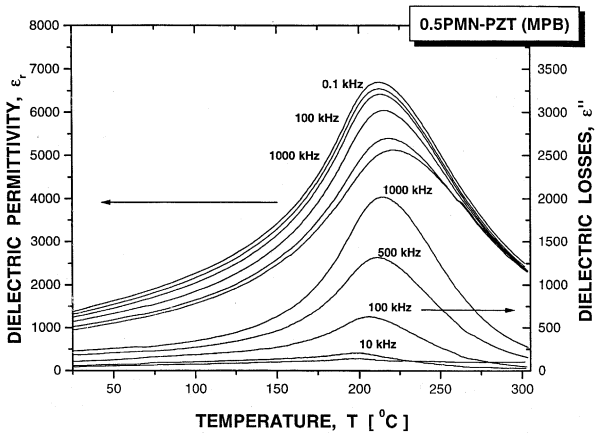

Fig. 6. Temperature dependencies of the relative dielectric permittivity and losses at four frequencies for $0.5Pb(Mg_{1/3}Nb_{2/3})O_3$–$0.5Pb(Zr_{0.47}Ti_{0.53})O_3$.

ferroelectric domain state and typical of a relaxor ferroelectric. This temperature is significantly higher than that of T_m (≈ -8 °C), indicating the presence of local polarization at temperatures far above T_m, and thus reflecting the presence of polar nanoregions above T_m. With decreasing temperature to −43 °C, an enhancement in the saturation polarization was observed, indicating an increase in the volume fraction of local polar regions. As temperature was further lowered to −120 °C, a typical ferroelectric type hysteresis loop became apparent in the polarization behavior. The loop has a sigmoidal shape, showing a relatively large remanent polarization $P_r \approx 7$ μC/cm^2 at zero field. This can be associated with the domain wall motion that switches domains and effects polarization.

Figs. 10a,b show the P–E curves for B-series materials with $x = 0.125$ and 0.5. Both samples exhibited a slight ferroelectricity at room temperature, similarly to pure PMN ceramics. A "slim" loop, as shown in Fig. 10 is typical of a phase with a suppressed long-range coulomb interaction. These results are consistent with the conjecture that $Mg_{1/3}Nb_{2/3}$ induces disorder into PZT.

It should be noted, comparing the values of P_r for all studied ferroelectric samples, that the remanent polarization of the composition with $x = 0.125$ near the MPB is the highest. It is well known that the polarization vector of the coexistence phase has 14 directions for dipole moment reorientation. The existence of a pseudocubic

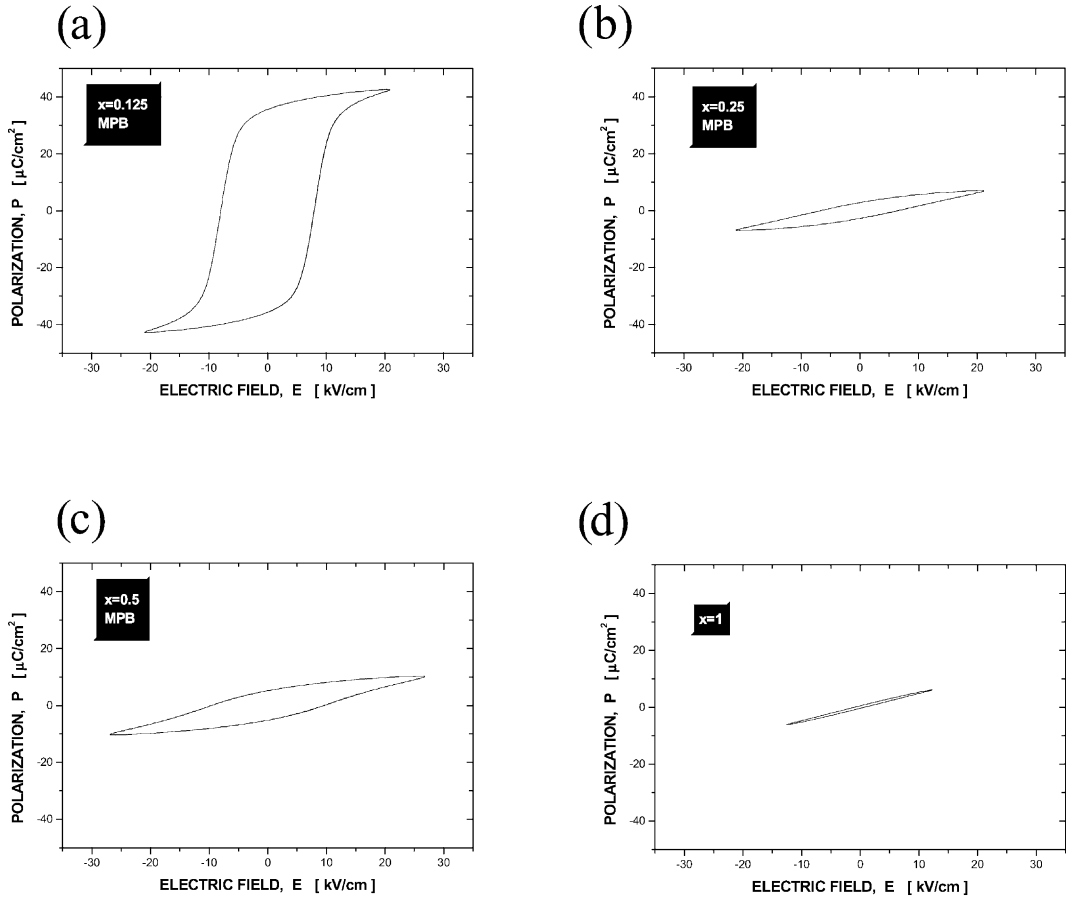

Fig. 7. Dielectric hysteresis loops of xPMN–(1−x)PZT with the composition near the MPB. (a) $x = 0.125$, (b) $x = 0.25$, (c) $x = 0.5$, (d) $x = 1$.

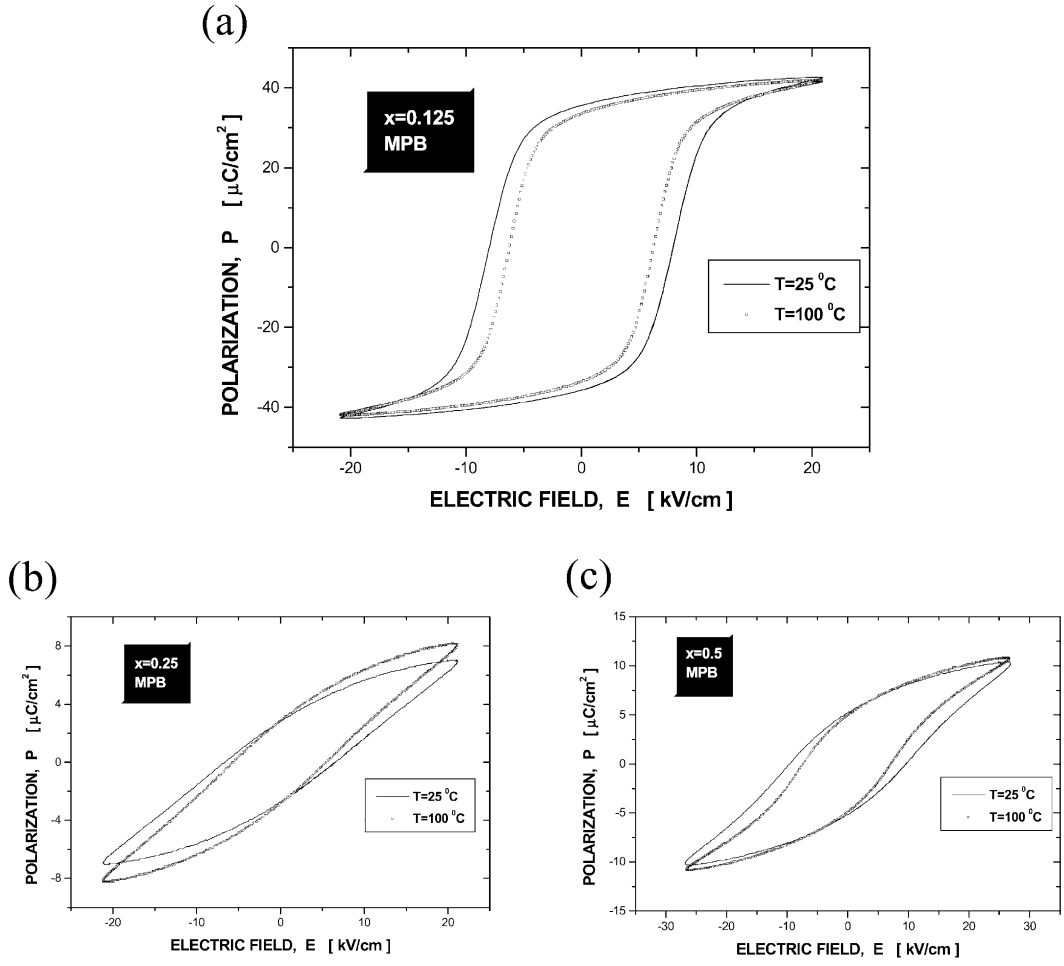

Fig. 8. Dielectric hysteresis loops measured at 25 and 100 °C for xPMN–(1−x)PZT with the composition near the MPB. (a) $x=0.125$, (b) $x=0.25$, (c) $x=0.5$.

phase in PMN2, PMN3 and PMN3P reduced significantly the remanent polarization of ferroelectrics. Long-range ferroelectric order is more easily induced under electric field for PMN1 ($E_c=8$ kV/cm) than that for other MPB compositions ($E_c=10$–12 kV/cm) containing a large amount of the pseudocubic phase. When the Ti:Zr ratio was increased, the phase structure transformation resulted in the decreasing coercivity.

From the extrapolation of the above results, as expected, PMN–PZT ternary solid solution is found to be ferroelectric, and furthermore to be a relaxor ferroelectric. The relaxor ferroelectric behavior of dielectric permittivity in PMN–PZT is shown in Fig. 6, and the field-dependent hysteresis behavior as another manifestation of the relaxor behavior is given in Fig. 10b.

3.4. Piezoelectric properties

Table 2 represents the effect of PMN modification on the piezoelectric properties, that is radial planar coupling factor (k^p), mechanical quality factor (Q_m), and piezoelectric d_{31} and d_{33} coefficients for xPMN–(1−x)PZT ceramic system with $x=0.125$, 0.25 and 0.5.

K^p, d_{33} And $|d_{31}|$ exhibited the maximum, $k^p=40\%$, $d_{31}=-106$ pC/N and $d_{33}=430$ pC/N at $x=0.125$, and then were decreased in proportion to the amount of PMN added in both compositional series. The decreasing in k^p and d_{31} can be attributed to the lower polarization of the materials, as deduced from the ferroelectric measurements. On the other hand, an increasing amount of $Mg_{1/3}Nb_{2/3}$ concentration resulted in increasing of Q_m. In general, for the same PMN content in the solid solution system, lower mechanical quality factor was found for the compositions close to the MPB.

The temperature behavior of k^p as well as d_{31} and d_{33} is similar, piezoelectric parameters decrease with increasing temperature up to the ferro-paraelectric transition temperature, as a result of the thermal evolution of ferroelectric polarization.

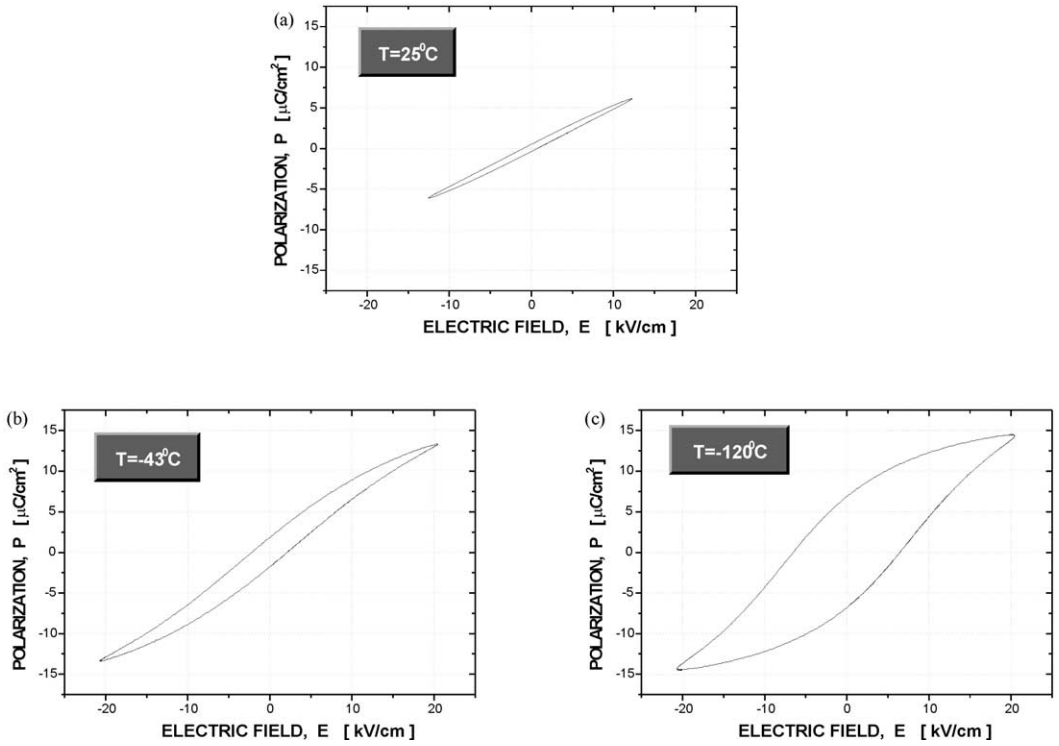

Fig. 9. Thermal evolution of P–E loops of $Pb(Mg_{1/3}Nb_{2/3})O_3$. (a) 25 °C ($T > T_m$), (b) −43 °C, (c) −120 °C.

4. Conclusions

The effect of PMN modification on the structural, dielectric, ferroelectric and piezoelectric properties of xPMN–(1−x)PZT ternary solid solution system ($x = 0.125, 0.25, 0.5$) was investigated. To distinguish the influence of Ti:Zr ratio variation, that is related to the maintenance of the MPB composition, two series materials having the nominal composition near the morphotropic transformation and a fixed Ti:Zr ratio, respectively, were synthesized by a columbite precursor method.

The following conclusions were made from the present study:

1. With increasing PMN content, a structural change from the tetragonal to pseudocubic phase was found in the composition range of $x = 0.125$–0.5 for $x Pb(Mg_{1/3}Nb_{2/3})O_3$–$(1-x)Pb(Zr_{0.47}Ti_{0.57})O_3$ system. The grain structure of both A- and B-series materials is fine, and additionally very heterogeneous in a case of $x = 0.5$. The pyrochlore phase was evidenced in xPMN–(1−x)PZT ternary system and its fraction over the perovskite phase increased as x increased.
2. For the MPB compositions of xPMN–(1−x)PZT ceramic system, the highest values of the dielectric constants as well as the piezoelectric and ferroelectric parameters showed a material with a low PMN content ($x = 0.125$). The introduction of PMN in compositions with a fixed Ti:Zr ratio of 53:47 resulted in increased dielectric permittivity maximum, whereas the electromechanical properties have been decreased due to an increased pseudocubic non-ferroelectric phase content. The temperature of dielectric permittivity maximum decreased as the amount of PMN

Table 2
Piezoelectric parameters of xPMN–(1−x)PZT ceramics

Sample	T [°C]	k^p	$d_{31} \times 10^{-12}$ [C/N]	$d_{33} \times 10^{-12}$ [C/N]	Q_m
PMN1	25	0.40	−106.1	430	71.4
	100	0.37	−118.7	–	57.7
	200	0.31	−124.1	–	69.1
PMN2	25	0.28	−58.7	208	115.5
	100	0.20	−46.0	–	81.4
	200	0.11	−31.7	–	178.7
PMN3	25	0.26	−58.5	121.0	121.0
	100	0.19	−51.6	–	93.5
	200	0.07	−21.2	–	181.5
PMN1T	25	0.29	−62.3	240	100.0
PMN2M	25	0.28	−58.7	208	115.5
PMN3P	25	0.19	−33.6	100	184.7

T—temperature, k^p—planar coupling factor, d_{33} and d_{31}—piezoelectric constants, Q_m—mechanical quality factor.

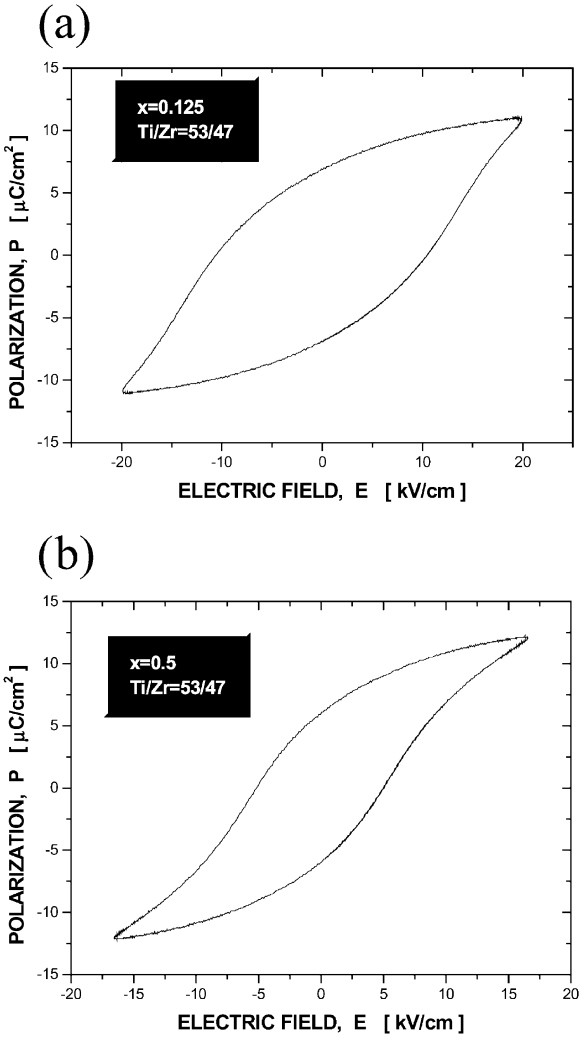

Fig. 10. Hysteresis loops of xPb($Mg_{1/3}Nb_{2/3}$)O_3–(1−x)Pb($Zr_{0.47}Ti_{0.53}$)O_3 ceramics recorded at room temperature with a cycling frequency of 0.01 Hz. (a) $x=0.125$, (b) $x=0.5$.

increased for both compositional systems of xPMN–(1−x)PZT. All investigated samples exhibited a diffuse phase transition behavior, however, the relaxor features were observed only for 0.5Pb($Mg_{1/3}Nb_{2/3}$)O_3–0.5Pb($Zr_{0.47}Ti_{0.53}$)O_3.

3. The measurement of hysteresis loops has revealed that the PMN in ternary xPMN–(1−x)PZT solid solution substantially suppresses long-range co-operation between ferroelectrically active dipoles. While the room-temperature state of 0.125 PMN–PZT with a composition near the MPB was confirmed to be long-range ordered ferroelectric, that of 0.5 PMN–PZT with Ti:Zr = 53:47 demonstrated typical of a relaxor ferroelectric. The presence of a pseudocubic phase in the system also significantly reduced a piezoelectricity.

Acknowledgements

This work was supported by the Grant Agency of the Slovak Academy of Sciences through Grant No. 2/2084/22.

References

1. Whatmore, R. W., Ferroelectrics, microsystems and nanotechnology. *Ferroelectrics*, 1999, **255**, 179–192.
2. Setter, N. and Waser, R., Electroceramic materials. *Acta Mater.*, 2000, **48**, 151–178.
3. Li, J. F., Dai, X., Chow, A. and Viehland, D., Polarization switching mechanisms and electromechanical properties of La-modified lead zirconate titanate ceramics. *J. Mater. Res.*, 1995, **10**(4), 926–938.
4. Baosong, W., Wenjun, S. and Jihua, M., Polar microdomain in relaxor ferroelectric ceramics and its electrostrictive effect. *Ferroelectrics*, 1997, **195**, 145–148.
5. Yokosuka, M., Ferroelectricity and phase transformations in $Pb(Mg_{1/3}Nb_{2/3})O_3$–$PbZrO_3$ solid solution ceramics. *Jpn. J. Appl. Phys.*, 1998, **37**(9B), 5257–5260.
6. Villegas, M., Caballero, A. C., Moure, C., Durán, P. and Fernández, J. F., Influence of processing parameters on the sintering and electrical properties of $Pb(Zn_{1/3}Nb_{2/3})O_3$-based ceramics. *J. Am. Ceram. Soc.*, 2000, **83**(1), 141–146.
7. Kondo, M., Hida, M., Tsukada, M., Kurihara, K. and Kamehara, N., Piezoelectric properties of $PbNi_{1/3}Nb_{2/3}O_3$–$PbTiO_3$–$PbZrO_3$ ceramics. *Jpn. J. Appl. Phys.*, 1997, **36**(9B), 6043–6045.
8. Akbas, M. A. and Davies, P. K., Thermally induced coarsening of the chemically ordered domains in $Pb(Mg_{1/3}Nb_{2/3})O_3$ (PMN)-based relaxor ferroelectrics. *J. Am. Ceram. Soc.*, 2000, **83**(1), 119–123.
9. Lin, H. T., Van Aken, D. C. and Huebner, W., Modeling the dielectric response and relaxation spectra of relaxor ferroelectrics. *J. Am. Ceram. Soc.*, 1999, **82**(10), 2698–2704.
10. Cross, L. E., Relaxor ferroelectrics. *Ferroelectrics*, 1987, **76**, 241–267.
11. Egami, T., Teslic, S., Dmowski, W., Viehland, D. and Vakhrushev, S., Local atomic structure of relaxor ferroelectric solids determined by pulsed neutron and X-ray scattering. *Ferroelectrics*, 1997, **199**, 103–113.
12. Cheng, Z. Y., Katiyar, R. S., Yao, X. and Guo, A., Dielectric behavior of lead magnesium niobate relaxors. *Phys. Rev. B*, 1997, **55**(13), 8165–8174.
13. Levstik, A., Kutnjak, Z., Filipič, C. and Pirc, R., Glassy freezing in relaxor ferroelectric lead magnesium niobate. *Phys. Rev. B*, 1998, **57**(18), 11204–11211.
14. Ouchi, H., Nagano, K. and Hayakawa, S., Piezoelectric properties of $Pb(Mg_{1/3}Nb_{2/3})O_3$–$PbTiO_3$–$PbZrO_3$ solid solution ceramics. *J. Am. Ceram. Soc.*, 1965, **48**(12), T26–T31.
15. Tsotsorin, A. N., Gridnev, S. A., Rogova, S. P. and Luchaninov, A. G., Dielectric and electromechanical properties of ceramic solid solutions $PbMg_{1/3}Nb_{2/3}O_3$–$PbZr_0Ti_{0.47}O_3$. *Ferroelectrics*, 1999, **235**, 171–180.
16. Swartz, S. L. and Shrout, T. R., Fabrication of perovskite lead magnesium niobate. *Mater. Res. Bull*, 1982, **17**, 1245–1250.
17. Alemany, C., González, A. M., Pardo, L., Jiménez, B., Carmona, F. and Mendiola, J., Automatic determination of complex constants of piezoelectric losy materials in the radial mode. *J. Phys. D: Appl. Phys.*, 1995, **28**, 945–956.